Electrosynthesized Reduced Graphene Oxide-Supported Platinum, Platinum-Copper and Platinum-Nickel Nanoparticles on Carbon-Ceramic Electrode for Electrocatalytic Oxidation of Ethanol in Acidic Media

Habibi, Biuck*+; Haghighi Shishavani, Yalda

Electroanalytical Chemistry Laboratory, Department of Chemistry, Faculty of Sciences, Azarbaijan Shahid Madani University, P.O. Box 53714-161 Tabriz, I.R. IRAN

ABSTRACT: *In this work, the electrocatalytic oxidation of ethanol was studied in acidic media at the wholly electrosynthesized nanocomposites: platinum and its alloys (copper and nickel) nanoparticles/reduced graphene oxide on the carbon-ceramic electrode (Pt/rGO/CCE, Pt-Cu/rGO/CCE, and Pt-Ni/rGO/CCE electrocatalysts). The electrosynthesized nanocomposites were characterized by scanning electron microscopy, X-ray powder diffraction, and energy-dispersive X-ray spectroscopy. Electrocatalytic activities of the Pt/rGO/CCE, Pt-Cu/rGO/CCE and Pt-Ni/rGO/CCE toward ethanol oxidation were investigated via cyclic voltammetric and chronoamperometric techniques in 0.1 M H_2SO_4 solution containing 0.3 M ethanol. The obtained results show that the Pt-Ni/rGO/CCE was catalytically more active and exhibits better electrocatalytic performance toward ethanol oxidation (ECSA=25.28, Jpf=0.156 mA/cm^2, Jpf/Jpb=1.12 and E_{onset}=0.2 V) than Pt-Cu/rGO/CCE (ECSA=19.09, Jpf=0.108 mA/cm^2, Jpf/Jpb=0.99 and E_{onset}=0.3 V) and Pt/rGO/CCE (ECSA=28.28, Jpf=0.092 mA/cm^2, Jpf/Jpb=0.55 and E_{onset}=0.35 V). The result of some effective and important investigational factors was studied and optimize conditions were suggested. Based on the obtained data one can be expected that the studied systems are promising systems for ethanol fuel cell applications.*

KEYWORDS: *Pt alloys; Reduced graphene oxide; Nanocomposite; Carbon-ceramic electrode; Electrooxidation; Ethanol; Fuel cell.*

INTRODUCTION

Over the past three decades, an increasing interest can be observed in research centers for the innovation and development of alternative power sources, for both weather and environmental reasons and the low availability of fossil fuels [1-4]. Reported results indicate that the Direct Alcohol Fuel Cells (DAFCs) [5, 6] have been regarded as one of the most appropriate and perspective choices as an alternative power source to fossil fuels [7].

** To whom correspondence should be addressed.*
+ E-mail: B.Habibi@azaruniv.ac.ir ; biuckhabibi_a@yahoo.com
1021-9986/2019/3/167-181 15/$/6.05

Among different types of direct alcohol fuel cells, methanol and ethanol fuel cells are suitable to power sources due to their high energy density, low working temperature, low pollutant emission, and ease of production and management of the liquid alcohols [8, 9]. Experiences in research centers have been shown that the direct ethanol fuel cells work much like direct methanol fuel cells [10]. However, ethanol is a hydrogen-rich liquid (6H per molecule), less toxic and has a higher specific energy (8.0 kWh/kg which corresponds to $12e^-$ per molecule for total oxidation) compared to methanol (6.1 kWh/kg) [11]. Also, ethanol can be obtained through a fermentation process in large scale from renewable resources like sugar cane, wheat, corn, or even straw [12].

Slow electro-kinetic properties of ethanol oxidation due to the breaking of the C-C bond for a total oxidation to CO_2 process and/or its partial oxidation are the major problems in electrocatalysis development and achieving high efficiency of electrooxidation reaction need to be introducing capable heterogeneous or homogenies electrocatalyst materials to increase the rate of electrochemical reaction [13]. It is well known that the Pt-based catalysts are the most active electrocatalyst for energy conversion and production via fuel cell technology [14]. However, the electrocatalytic activity of pure and smooth Pt for ethanol oxidation is limited because Pt will be easily poisoned by intermediate species such as CO during the electrooxidation process [15] and also it is highly expensive, so it is necessary to decrease the use of Pt and improve its efficiency [16]. Therefore, it is required to design new form of Pt based electrocatalysts to improve the kinetic of ethanol oxidation and also to find capable supports for such electrocatalysts to reduce their amount and cost [17-27]. On the other hand, poisoning of effect of the CO on the Pt particles can be efficiently decreased through surface reaction with neighboring OH_{ads} species electrosorbed from water oxidation [28]. So, alloying of Pt atoms with oxophilic metals provides OH_{ads} species on second metal sites at more negative potentials compared with pure Pt and, therefore, allows electrocatalytic oxidation of CO at lower anodic overpotentials. Among these alloys, bimetallic Pt-M (M=Ni, Cu, Ru and …) electrocatalysts have been demonstrated to exhibit attractive electroactivity [6, 8, 13, 17, 18, 20-26]. A survey in the literature shows that the Pt alloy nanoparticles have been widely used as electrocatalysts for ethanol oxidation [29-39]. Alternatively, the choice of a suitable supporting material is an imperative factor that may affect the performance and consumable of the supported Pt-based electrocatalysts owing to their interactions and surface reactivity's [33-41]. In fact, physicochemical characteristics and surface chemistry of a support material influence the properties and performance of supported electrocatalysts [42-44]. The support material can assist the formation of highly distributed electrocatalyst nanoparticles with small and tunable size, narrow size distribution and consequently reduces their consumption and increases their efficiency and improves the performance [2, 8, 14, 26, 30, 32, 33-38, 40-44]. Carbon materials as support are of special interest due to their outstanding properties, such as their tunable shape, size, porosity, chemical stability, corrosion resistance, low cost, good thermal resistance, and electrical conductivity [[33-38, 40-44]. Graphene, one-atom thick planar sheet of carbon atoms, and its families have been attracted tremendous scientific attention in recent years [33-38, 45-50]**.** Graphene family's exhibit superior electrical conductivity and extremely high specific surface area, and therefore, graphene and their families should be explored as suitable support materials to improve electrocatalytic activities of electrocatalyst nanoparticles for ethanol oxidations [33-38, 51, 52]. In recent years, reduced graphene oxide (rGO), one of the most famous members of the graphene family, is widely used as a support for electrocatalysts nanoparticles in ethanol electrooxidation reactions [33, 37, 49, 50, 53-62].

In this study, Pt, Pt-copper (Pt-Cu) and Pt-nickel (Pt-Ni) alloy nanoparticles are electrodeposited on/in electrosynthesized rGO layers supported on Carbon-Ceramic Electrode (CCE) and resulted nanocomposites are applied as the electrocatalysts for ethanol oxidation. The electrosynthesized nanocomposites (Pt/rGO, Pt-Cu/rGO, and Pt-Ni/rGO) are characterized by X-Ray powder Diffraction (XRD), Scanning Electron Microscopy (SEM) and Energy-Dispersive X-ray (EDX) spectroscopy. And then the electrocatalytic activities of Pt/rGO/CCE, Pt-Cu/rGO/CCE, and Pt-Ni/rGO/CCE are systematically investigated for ethanol oxidation in acid media. The result of some effective and important investigational factors is studied and optimize conditions are suggested. Based on the obtained results, one can be expected that

the studied systems are the promising systems for ethanol fuel cell applications.

EXPERIMENTAL SECTION

Chemicals

Methyltrimethoxysilane (MTMOS), methanol, ethanol, potassium permanganate, hydrogen peroxide, $H_2PtCl_6.5H_2O$, $CuCl_2.2H_2O$, $NiCl_6.6H_2O$, HCl, H_2SO_4 and graphite powder with high purity were obtained from Merck. All solutions were prepared with double distilled water.

Preparation of graphene oxide

Graphene Oxide (GO) was prepared according to Hummer's method [65]. Briefly, 5.0 g of thermally treated graphite powder was added to 115 mL H_2SO_4 98% in an ice bath. 15.0 g of potassium permanganate were gradually and with carefully controlled rate added in the ice bath with stirring of the solution to avoid sudden increase in temperature. The obtained mixture was kept at 35 °C for 30 min and then 230 mL of double deionized water was slowly added to the product container, causing increase in temperature to 98 °C. After 15 min, the mixture was further treated with 700 mL of double deionized water and 50 mL of 30% H_2O_2 solution, respectively. GO as final product was separated and then washed with double deionized water for several times to remove residuals until pH reached to 7 and finally dried it at 65 °C in a vacuum oven.

Preparation of Pt/rGO, Pt-Cu/rGO, and Pt-Ni/rGO modified carbon-ceramic electrodes

Carbon-Ceramic Electrode (CCE) as a homemade substrate was constructed [60, 62, 65, 66, 75] based on the sole-gel processing method according to the following procedure: The amount of 0.9 mL MTMOS as precursor was mixed with 0.6 mL methanol. Then, 0.6 mL HCl 0.1 M was added as a catalyst and the mixture was magnetically stirred (for about 15 min) until a clear and homogeneous solution was produced. Then, 0.3 g graphite powder was added and the mixture was shaken for another 5 min. Subsequently, the homogenies mixture was firmly packed into a Teflon tube (with 3 mm inner diameter and 10 mm length) and dried for at least 24 h at room temperature. A copper wire was inserted through the other end of tube to set up electric contact.

Preparation of the Pt/rGO/CCE: The CCE surface was polished with 1500 emery paper to obtain a smooth surface and rinsed with double distilled water. Cyclic voltammetry was used for electrochemical deposition of rGO nanosheets on the CCE from 1.0 mg/mL GO in aqueous 0.07 M phosphate buffer pH=8.5 solution as the supporting electrolyte. Fig. 1 shows the consecutive Cyclic Voltammograms (CVs) of GO reduction on the CCE in 0.07 M phosphate buffer solution pH=8.5. As can be seen in Fig. 1, during forwarding first potential scan an anodic peak (a_1) in -0.4 V versus Saturated Calomel Electrode (SCE) and in reverse potential scan two cathodic peaks (c_1, c_2) in -0.65, -0.8 V versus SCE have appeared. Peaks of a_1 and c_1 corresponding to oxidation and reduction of oxygen-containing groups on the GO respectively [62, 63]. With consecutive scans, the currents of a_1 and c_1 peaks were increased which represents electrochemically deposition of rGO on CCE. Cathodic peak (c_2) corresponds to electrochemically reduction of GO and was disappeared in final cycle which represents GO fully reduced.

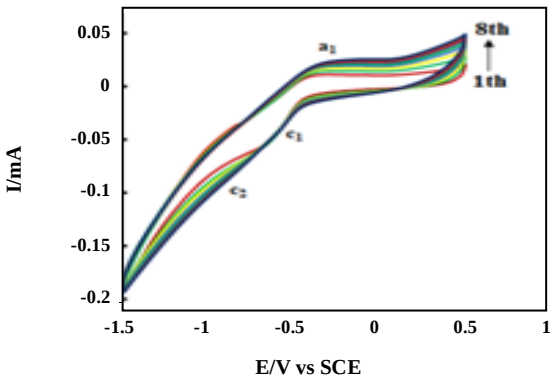

Fig. 1: Consecutive CVs (eight cycles) of CCE in 0.07 M phosphate buffer solution (pH=8.5) containing 1.0 mg/mL GO.

After drying the rGO/CCE, the Pt nanoparticles were electrochemically deposited on the rGO/CCE from 1.0 mM H_2PtCl_6 in aqueous 0.1 M H_2SO_4 solution as the supporting electrolyte [65].

Preparation of Pt-Cu/rGO/CCE: As above, after polishing of the CCE, the rGO nanosheets were electrodeposited on the CCE to prepare of rGO/CCE. Then the Pt-Cu alloy nanoparticles were electrodeposited [potentiostatically at -0.3 V versus (SCE)] on the rGO/CCE from an aqueous solution of 0.1 M H_2SO_4 containing H_2PtCl_6 and $CuCl_2$ (total concentration of two salts equal to 1.0 mM with 2:1 ratio) at 25 °C.

Preparation of Pt-Ni/rGO/CCE: This electrocatalyst was prepared by the same above process. Just, the Pt-Ni alloy nanoparticles were electrodeposited [potentiostatically at -0.3 V versus (SCE)] on/in the rGO/CCE from an aqueous solution of 0.1 M H_2SO_4 containing H_2PtCl_6 and $NiCl_2$ (total concentration of two salts equal to 1.0 mM with 2:1 ratio) at 25 ^oC.

Instrumentation

The electrochemical tests were carried out by utilizing an AUTOLAB PGSTAT-100 (potentiostat/galvanostat) equipped with a USB electrochemical interface and driven GEPS software. A conventional three-electrode cell contains: the nanocomposite modified electrodes (Pt-rGO/CCE, Pt-Cu/rGO/CCE and Pt-Ni/rGO/CCE), SCE and a Pt wire respectively as the working, reference, and auxiliary electrodes were used at room temperature. JULABO thermostat was used to control cell temperature. SEM and EDX experiments were performed on a LEO 440i Oxford instrument. XRD patterns was obtained using a Brucker AXF (D8 Advance) X-ray power diffractometer with a Cu-Ka radiation source (l=0.154056 nm) generated at 40 kV and 35 mA.

RESULTS AND DISCUSSION

Physical characterization

The crystallographic structure of the prepared electrocatalysts was investigated by XRD patterns. The XRD patterns of the Pt/rGO/CCE, Pt-Cu/rGO/CCE and Pt-Ni/rGO/CCE are shown in Fig. 2 (a-c respectively). There are two typical diffraction peaks at 2θ = 26.6° and 55° in all patterns which can be attributed to supporting carbonic material (graphite powder) (002) and (006), respectively. The diffraction peaks at 2θ = 40.2°, 46.5°, and 68.3° (pattern a in Fig. 2) can be assigned to the characteristic planes of Pt (111), (200) and (220) in Pt/rGO/CCE. The XRD patterns of the Pt-Cu/rGO/CCE and Pt-Ni/rGO/CCE in Fig. 2 (pattern b and c) present also the main characteristic peaks of the face-centered cubic (fcc) crystalline Pt at 2θ = 41.5, 46.8 and 68.3, namely, the planes (111), (200) and (220). The slight shifts of the Pt diffraction peaks in the Pt-Cu/rGO and Pt-Ni/rGO reveals the formation of the alloy due to the incorporation of Cu and Ni atoms into the fcc structure of Pt [66, 67]. Also as can be seen in the Fig. 2 patterns b and c, absence of any distinct reflection peaks due

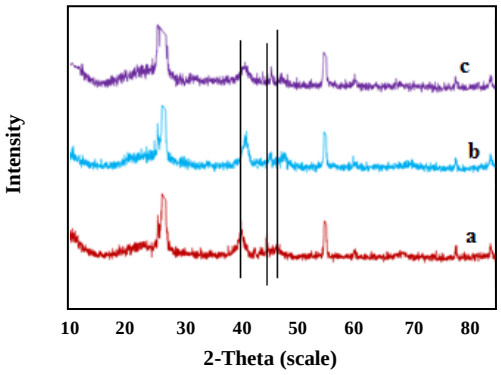

Fig. 2: XRD patterns of Pt/rGO/CCE (a), Pt-Cu/rGO/CCE (b), and Pt-Ni/rGO/CCE (c).

the presence of Cu and Ni atoms than those of the above mentioned peaks indicates that these electrocatalysts have prevailed Pt (fcc) crystal structure [68, 69].

Surface morphology and chemical structural characterization of Pt/rGO/CCE, Pt-Cu/rGO/CCE, and Pt-Ni/rGO/CCE were investigated by SEM and EDX. The SEM images of Pt/rGO, Pt-Cu/rGO and Pt-Ni/rGO nanocomposites on the CCE are presented in Fig. 3 (a), (c) and (e), respectively. The high magnification of SEM images of Pt/rGO, Pt-Cu/rGO, and Pt-Ni/rGO nanocomposites are also shown in Fig. 3 (b), (d) and (f), respectively. Fig. 3 image k shows the SEM of the rGO/CCE surface. As can be seen, the surface of CCE is completely protected by rGO layers and is favorable for electrodispersion of metallic nanoparticles. According to Fig. 3 (a, b), it could be seen that cauliflower like Pt nanoparticles exhibits very well uniform spreading and homogeneously range in size. Fig. 3 image c and d show SEM and high magnification SEM images of Pt-Cu/rGO/CCE. It can be seen that cypress form of Pt-Cu nanoparticles has dendrimer mode and are in an average diameter of 20 nm.

Fig. 3 images d and f show the cluster form of the Pt-Ni nanoparticles with small size and narrow size distribution. Parts (g), (h) and (i) show the EDX spectrums of Pt/rGO/CCE, Pt-Cu/rGO/CCE and Pt-Ni/rGO/CCE, respectively. As shown in Fig. 3 part (g), two main peaks assigned to C (related to the substrate) and also two key peaks of Pt atoms can be observed. On the other hand, in Fig. 3 (h, i), it is evident that Pt, Cu, and Ni atoms are present on the nanocomposites. The presence

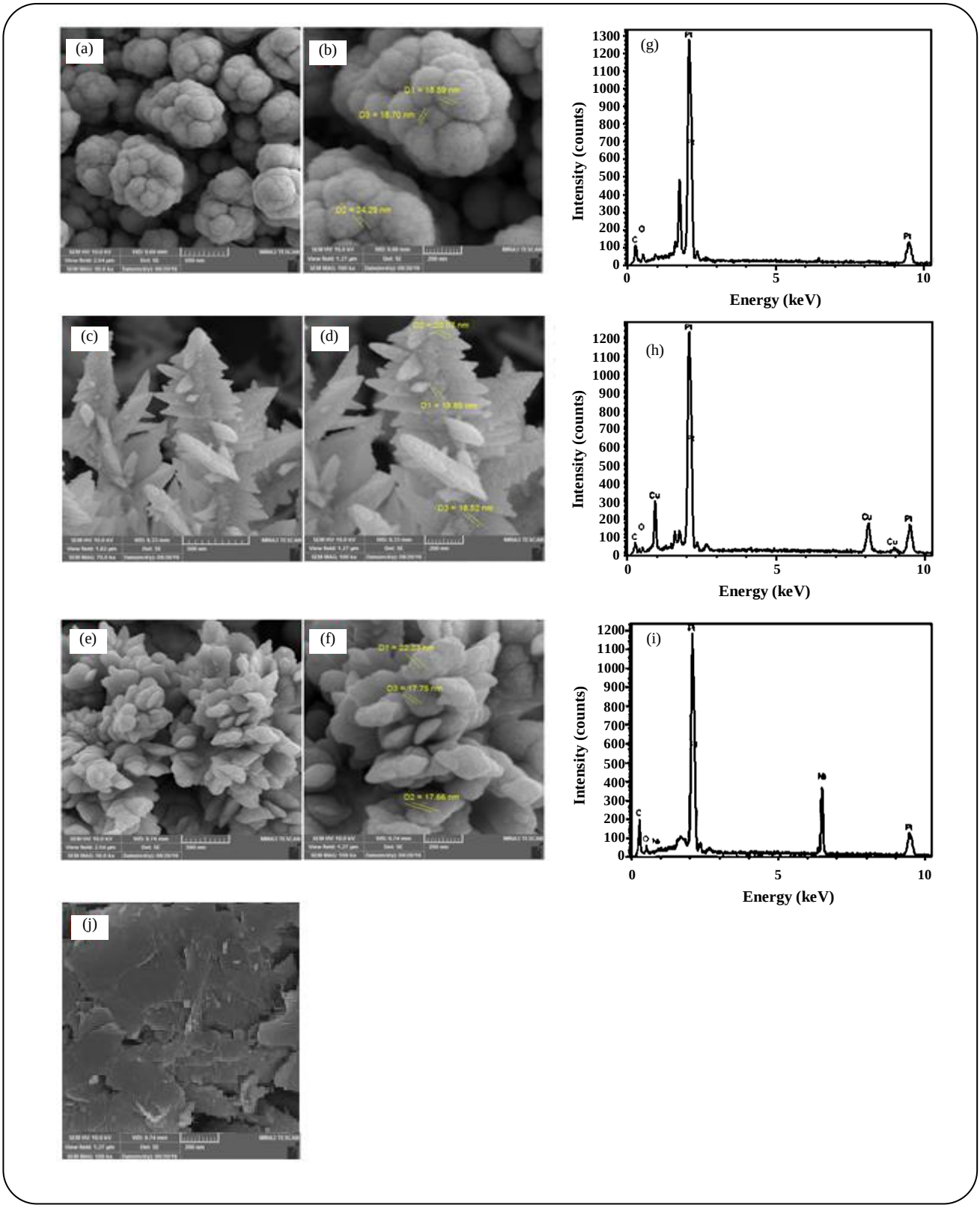

Fig. 3: SEM images of Pt/rGO/CCE (a), Pt-Cu/rGO/CCE (c), Pt-Ni/rGO/CCE (e), high magnification SEM images of Pt/rGO/CCE (b), Pt-Cu/rGO/CCE (d), Pt-Ni/rGO/CCE (f), SEM image of rGO/CCE (j), EDX spectrum of Pt/rGO/CCE (g), Pt-Cu/rGO/CCE (h), Pt-Ni/rGO/CCE (i).

of small oxygen peak in Fig. 3 (g-i) means that rGO contains a small amount of carboxyl and hydroxyl group and implies that the GO was converted into rGO in the electrochemical deposition process.

Electrochemical characterization

Fig. 4 shows the CVs of Pt-Cu/rGO/CCE and Pt-Ni/rGO/CCE electrocatalysts in an acidic media (0.1 M H_2SO_4 aqueous solution) within the potential range of -0.3 and 1.3 V at a scan rate of 50 mV s^{-1}. As can be seen in Fig. 4, whole profile of both CVs contain three pairs of anodic and corresponding cathodic peaks (I/I', II/II' and III/III') in the scanned potential range. Form the left direction, the first two couples (I/I' and II/II') at negative potentials region (-0.3 to 0 V) are correspond to the adsorption/desorption of hydrogen (weak and strong adsorption/desorption state) on the electrocatalyst nanoparticles, while the third pair (III/III') that appeared in positive potentials region (0.3 to 1.3 V) corresponds to the formation of a different form of Pt oxide and their reduction in negative scans, respectively [50]. Inset of Fig. 4 shows the CV of Pt/rGO/CCE in the same conditions for comparison. According to Fig. 4 and its inset, the current of adsorption/desorption of hydrogen are reduced in Pt-Cu/rGO/CCE and Pt-Ni/rGO/CCE electrocatalysts in comparison with Pt/rGO/CCE due to the reduction of their Pt amount [50, 55, 56, 58]. It is clear that the electrocatalytic activities of an electrocatalyst are expected to depend on the number of available active surface sites. On the other hand, electrocatalytic activities referred to real Pt nanoparticle surface area have a clear physical significance in their performance evaluation [8, 70]. Always, the electrochemical surface area (ECSA) of an electrocatalyst is defined as the measure of the number of electrochemically active sites per milligram of electrocatalysts [6, 11, 36-39]. Measurement of electric charge related to the hydrogen adsorption peaks is widely used for estimating of the ECSA [69, 70-72]. The ECSAs of Pt/rGO/CCE, Pt-Cu/rGO/CCE, and Pt-Ni/rGO/CCE have estimated by calculation of electric charge of the hydrogen adsorption peaks area (Q_H) according to Equation (1):

$$ECSA = Q_H/[Pt]\ 0.21 \quad (1)$$

Where [Pt] in mg represents the Pt loading in the electrocatalyst, Q_H represents the electric charge in mC

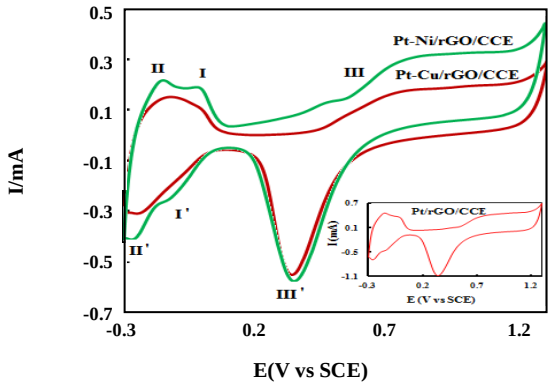

Fig. 4: CVs of Pt-Cu/rGO/CCE and Pt-Ni/rGO/CCE electrocatalysts in 0.1 M H_2SO_4 at a scan rate of 50 mV/s (25°C). Inset is the CV of Pt/rGO/CCE in the same conditions.

that was measured form the hydrogen adsorption peaks area and the constant 0.21 (mC cm^{-2}) represents the maximum surface charge transferred to Pt during the adsorption of hydrogen monolayer [70-72]. The calculated values of ECSAs for the present electrocatalysts along with smooth Pt are listed in Table 1. These ECSA values of the electrocatalysts are in order of Pt/rGO/CCE>Pt-Ni/rGO/CCE>Pt-Cu/rGO/CCE>Smooth Pt.

Electrocatalytic activity for ethanol electrooxidation reaction

The catalytic activity of present electrocatalysts was investigated by cyclic voltammetry in the solution of ethanol (0.3 M)/H_2SO_4 (0.1 M) at a scan rate 50 mV/s. Fig. 5 shows the CVs of ethanol electrooxidation on the Pt/rGO/CCE (a), Pt-Cu/rGO/CCE (b) and Pt-Ni/rGO/CCE (c), respectively. During the forward scan, there are two oxidation peaks in the profiles of the all CVs: these two anodic peaks at potentials about 0.6 V and 1.1 V correspond to direct electrooxidation of the two kinds of chemisorbed species of this fuel at the surface of the electrocatalyst that can be assigned to the total ethanol oxidation (process 2 in the below) in this condition. Several electrochemical and spectroscopic investigations [13, 29, 73, 74] have been reported on the electrooxidation of ethanol in acid solution and based on their results, the following mechanisms have been suggested according to the parallel reactions:

$$CH_3CH_2OH \rightarrow [CH_3CH_2OH]_{ads} \rightarrow \quad (2)$$

$$C_{1ads}; C_{2ads} \rightarrow CO_2 \qquad \text{total oxidation}$$

Table 1: Comparison of ECSA values for smooth Pt, Pt/rGO/CCE, Pt-Cu/rGO/CCE and Pt-Ni/rGO/CCE.

Electrocatalyst	smooth Pt	Pt/rGO/CCE	Pt-Cu/rGO/CCE	Pt-Ni/rGO/CCE
ECSA	0.39	28.28	19.09	25.28

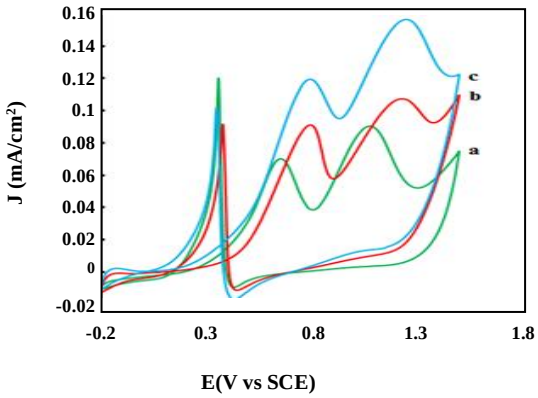

Fig. 5: CVs of 0.3 M ethanol on the Pt/rGO/CCE (a), Pt-Cu/rGO/CCE (b) and Pt-Ni/rGO/CCE (c) in 0.1 M H_2SO_4 at scan rate of 50 mV/s.

$$CH_3CH_2OH \rightarrow [CH_3CH_2OH]_{ads} \rightarrow \quad (3)$$
$$CH_3CHO \rightarrow CH_3COOH \qquad \text{partial oxidation}$$

In process 2, C_{1ads} and C_{2ads} represent the two adsorbed intermediates on the surface of electrocatalysts with one and two carbon atoms, respectively.

The other anodic peak (sharp and needle like) in the backward scan at about 0.4 V corresponds to the oxidation of intermediates which formed in the forward scan [53]. Comparison of CV a, b and c in Fig. 5 shows that the ethanol electrooxidation current densities at the Pt-Ni/rGO/CCE electrocatalyst (CV c) are higher than Pt/rGO/CCE (CV a) and also Pt-Cu/rGO/CCE (CV b) [6, 20, 48, 58, 60, 72]. I.e. the forward peak current densities of ethanol electrooxidation in this condition are as the following order:

Pt-Ni/rGO/CCE>Pt-Cu/rGO/CCE>Pt/rGO/CCE.

From Fig. 5, also, it can be observed that the onset potential of ethanol electrooxidation on the Pt-Ni/rGO/CCE, Pt-Cu/rGO/CCE and Pt/rGO/CCE electrocatalysts is about 0.2 V, 0.3 V and 0.35 V versus SCE, respectively. i.e., the onset potential of ethanol electrooxidation on the Pt-Ni/rGO/CCE is lower than those on the Pt-Cu/rGO/CCE and Pt/rGO/CCE electsocatalysts**.** These results indicate that the addition of Ni and Cu into Pt nanoparticles and formation of alloy can significantly improve the performance of electrocatalyst for the ethanol electrooxidation and signify that the Pt-Ni/rGO/CCE and Pt-Cu/rGO/CCE electrocatalysts are more active than Pt/rGO/CCE. However, the comparison of these two alloys shows that the Pt-Ni/rGO nanocomposite can significantly improve the electrocatalyst performance for the ethanol electrooxidation. On the other hand, the reverse anodic peak current densities are: Pt-Ni/rGO/CCE (0.107 mA/cm^2), Pt-Cu/rGO/CCE (0.096 mA/cm^2) and Pt/rGO/CCE (0.127 mA/cm^2). The ratio of the forward anodic peak current density (Jp_f) to the reverse anodic peak current density (Jp_b) can be used to describe the electrocatalyst tolerance to carbonaceous species such as CO [60, 62, 65, 66, 70]. Pt-Ni/rGO/CCE electrocatalyst has a ratio of 1.12 which is higher than Pt-Cu/rGO/CCE (0.99) and Pt/rGO/CCE (0.55), a result which suggests that the Pt-Ni/rGO/CCE electrocatalyst generate more complete oxidation of ethanol to carbon dioxide than others. These results again suggest that the presence of Ni and also Cu can decrease the barrier of the ethanol oxidation, and Pt-Ni/rGO nanocomposite have higher performance than Pt/rGO and also Pt-Cu/rGO nanocomposites. The effects of Cu and especially Ni elements at the present binary alloys in the enhancement of ethanol electrooxidation reaction rate can be reasonably explained based on the following triple reasons [33, 50, 55, 56, 58]: Firstly through the bifunctional mechanism, which should consider adsorption properties of CO and OH species on every component of alloy, secondly by the electronic interaction between the Pt and Ni (or Cu) element, and thirdly by the growth in ECSA due to the ‘‘leaching out’’ effect of the alloying element (Ni or Cu). According to the first factor, an efficient electrocatalyst facilitates CO desorption on Pt atoms by the formation of OH_{ads} on the Ni atoms. Therefore, CO adsorption mainly occurs on Pt, while OH_{ads} species easily interact with Ni or Cu atoms surface. Hence, the binary combination supplies the best overall activity and high kinetic for ethanol electrooxidation.

$$Ni \text{ or } Cu + H_2O \rightarrow NiOH_{ads} \text{ or } CuOH_{ads} + H^+ + e^- \quad (4)$$

Table 2: Comparison of the performance of the Pt-Ni/rGO/CCE electrocatalyst with others toward electrooxidation of ethanol in acidic solution.

Electrocatalyst	E_{onset} *	E_{pf}	E_{pb}	I_{pf} (mA cm^{-2})**	I_{pb} (mA cm^{-2})	I_{pf}/I_{pb}	Stability	Ref.
$Pt_{0.7}$-$Rh_{0.3}$ /$C_{25}(SnO_2{:}Sb)_{75}$	0.160	0.659	0.409	1.0(S_{Real})	0.95	1.05	600 s (0.09 mA cm^{-2})	17
Pt-NiO_x/C	0.449	0.64	-	1.68 (S_{Real})	-	-	3600 s (0.158 mA cm^{-2})	19
Pt_2Ni/C	0.282	0.815	0.509	0.53(S_{Real})	0.54	0.98	1800 s (0.07 mA cm^{-2})	20
$Pt_{2.3}Ni$/C	0.279	0.809	0.524	1.48 (S_{Real})	3.1	0.48	1800 s (0.2 mA cm^{-2})	20
Pt_3Co@Pt/PC	0.21	0.51	0.3	0.75 mA μg^{-1} Pt	0.6	1.25	-	22
PtSn/CNTs	0.41	0.88	0.75	1.36(S_{Real})	1.56	0.87	3600 s (20 mA mg^{-1} Pt)	26
Pt/Ta	0.4	0.7	0.37	19 mA	20.5	0.93	400 s (3 mA)	27
Pt_3Sn/GO	0.54	0.82	0.4	31 (S_{GeO})	20	1.55	3000 s (32 mA cm^{-2})	36
Pt-Ru-graphene	0.0	0.66	0.46	18.1	5.23	3.46	-	53
PtRuNi/FLG	0.31	0.8	0.47	1.08 mA mg^{-1} Pt	1.65	0.66	120 s (0.37 mA mg^{-1} Pt)	55
Pt-Ni/CCE	0.318	0.868	0.23	2.49(S_{Real})	1.5	1.66	-	60
Pt-Cu/RGO	0.25	0.68	0.4	0.75(S_{Real})	0.82	0.91	3000 s (0.07 mA cm^{-2})	61
Pt/CCE	0.1	0.62	0.37	34 (S_{GeO})	39	0.87	3000 s (8.4 mA cm^{-2})	75
Pt-Ni/rGO/CCE	0.2	0.8	0.3	0.156 (S_{Real})	0.14	1.12	1000 (2.6 mA cm^{-2})	This work

** vs SCE and **S_{Geo}= based on geometric surface area and S_{Real} based real surface area.*

$$NiOH_{ads} \text{ or } CuOH_{ads} + PtCO_{ads} \rightarrow CO_2 + Pt + Ni \text{ or } Cu + H^+ + e^- \quad (5)$$

In order for a comprehensive evaluation, a comparison of the designed electrocatalyst with previous related reports is necessary. To compare the electrocatalytic performance of the Pt-Ni/rGO/CCE toward ethanol oxidation in acidic media with other electrocatalysts,
the electrochemical parameters such as E_{onset}, E_{pf}, E_{pb}, I_{pf}, I_{pb}, I_{pf}/I_{pb} and stability obtained in this study and reported results were listed in Table 2.

Table 2 shows that the Pt-Ni/rGO/CCE displays better or comparable electrocatalytic performance in comparison with other reported electrocatalysts in ethanol oxidation.

Parameters affecting the ethanol electrooxidation

Ethanol concentration effect

In this section, the effect of ethanol (fuel) concentration on its electrooxidation and corresponding forward anodic peaks current density was investigated by cyclic voltammetry at the Pt/rGO/CCE, Pt-Cu/rGO/CCE and Pt-Ni/rGO/CCE electrocatalysts for the evaluation of their electrocatalytic capacity. According to the experimental results (not shown here), the forward anodic peaks current density of the ethanol oxidation on the Pt/rGO/CCE, Pt-Cu/rGO/CCE and Pt-Ni/rGO/CCE increased by increasing of its concentration and reached to nearly constant value at concentration higher than 1.5 M due to saturation of ECAS of the electrocatalysts.

Temperature effect

Temperature effect on the ethanol electrooxidation and corresponding forward anodic peaks current density at the Pt-Ni/rGO/CCE electrocatalyst in acidic media was investigated and the obtained results are shown in Fig. 6 A. With increasing temperature from 20 to 60 ºC, the CV currents rise by a factor of about 3. As can be seen in Fig. 6 B, the forward anodic peaks current density (first anodic peaks current density curve a and second anodic peaks current density curve b) of ethanol electrooxidation increase with increasing medium temperature up to 60 ºC. The incremental effect of medium temperature may be attributed to the (a) decreasing the CO coverage on the electrocatalyst nanoparticles surface with increasing temperature, (b) increasing of ethanol adsorption due to

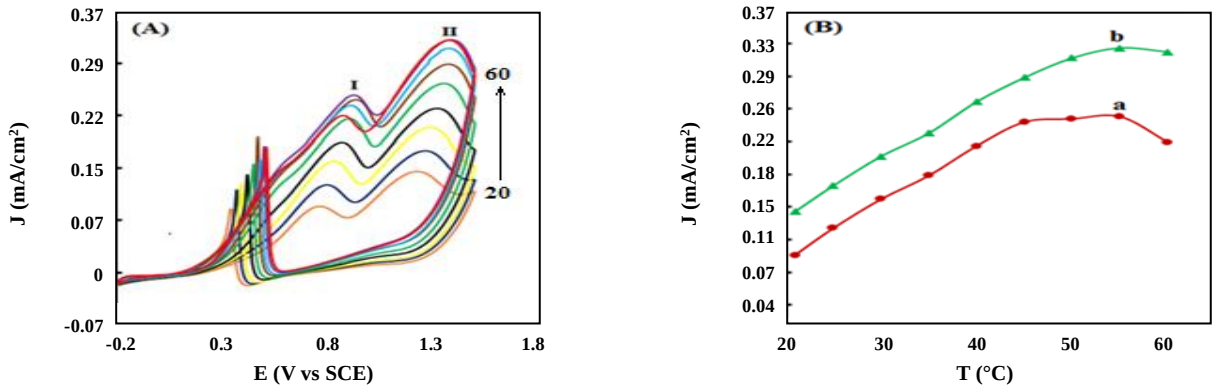

Fig. 6: CVs of the ethanol (0.3 M) electrooxidation at the Pt-Ni/rGO/CCE electrocatalyst in different temperatures (A) and plot of forwarding anodic peak current densities as a function of temperature [curve a for (peak I) and curve b for (peak II)] (B).

decreasing the CO coverage and resulting acceleration of the electrode reaction kinetics [75-78]. It should be noted that, in higher temperature (>60 ºC), the current densities of forwarding anodic peaks decrease with increasing of the medium temperature. This effect can be attributed to the progressive evaporation of ethanol at high temperatures. Same results were obtained for Pt/rGO/CCE and Pt-Cu/rGO/CCE.

Upper limit potentials (EU) (anodic reversal potential) effect

Fig. 7 shows the CVs of ethanol electrooxidation on the Pt-Ni/rGO/CCE electrocatalyst in different EU from 0.8-1.5 V. As can be seen in Fig. 7, by increasing the final upper positive potential limit, the changes in the CV profiles and peak current densities of the ethanol electrooxidation can be concluded as anodic peak current density and anodic peak potential in the forward scan remain approximately unchanged but the oxidation peak current density in the backward scan increase with increasing EU and finally decrease (Hill-like changes). As reported in the literature [76], oxidation peak in the backward scan is related to the oxidation of ethanol molecules, ethanol residues in reaction pathway and intermediates and potential depended products of ethanol electrooxidation [76, 77]. Same results were obtained for Pt/rGO/CCE and Pt-Cu/rGO/CCE electrocatalysts.

Scan rate effect

The effect of the scan rate on the ethanol electrooxidation at the Pt-Ni/rGO/CCE electrocatalyst was studied for obtaining the kinetic information. Fig. 8 shows the CVs

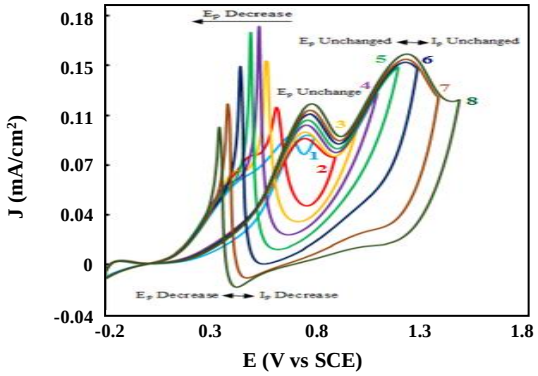

Fig. 7: CVs of ethanol (0.3 M) electrooxidation in 0.1 M H_2SO_4 at the Pt-Ni/rGO/CCE electrocatalyst in different upper limit potential: (1) -0.2 to 0.8 V, (2) -0.2 to 0.9 V, (3) -0.2 to 1.0 V, (4) -0.2 to 1.1 V, (5) -0.2 to 1.2 V, (6) -0.2 to 1.3 V, (7) -0.2 to 1.4 V and (8) -0.2 to 1.5 V, scan rate 50 mV/s.

of the ethanol electrooxidation at the Pt-Ni/rGO/CCE electrocatalyst at different scan rates. As can be seen, by increasing the scan rate the current density in all CVs was increased. Looking at the whole of CVs clearly reveal that the peak current of two main anodic peaks (I and II) in the forward scan, reduction peak (III) due to the reduction of different form of Pt oxides and oxidation peak (IV) in the backward scan increase linearly with the scan rate. Inset A in Fig. 8 (curve a and b) shows the plots of the peak currents of two main peaks as a function of the square root scan rate ($v^{1/2}$). As can be seen, the current values of main two anodic peaks are liner vs. $v^{1/2}$. Inset of B shows the peak current of main peaks [curve a (process I) and b (process II)] as function of scan rate. From

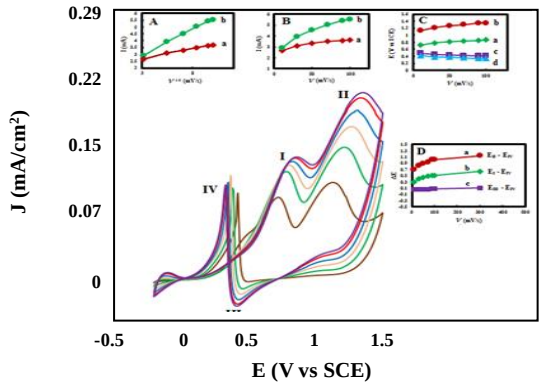

Fig. 8: CVs of ethanol (0.3 M) electrooxidation in 0.1 M H_2SO_4 at the Pt-Ni/rGO/CCE electrocatalyst in different scan rates. Plot of Ips for peak I and II versus square root of scan rate (curve a, b) (A), plot of Ips for same peaks versus scan rate (B), variation of peak potential of first anodic peak (I) (curve a), second anodic peak (II) (curve b), cathodic peak (III) (curve c), anodic peak (IV) (curve d) (C) and ΔE between of the peak potential of process I and IV (curve a), II and IV (curve b), III and IV (curve c) (D).

the curves in inset B, it can be seen that the peak current of the main peaks varies nonlinearly with scan rate. These behaviors indicate that the electrocatalytic processes are controlled by diffusion. For backward scan, in different scan rates the time and opportunity for poisoning species to adsorb on nanoparticles surface was chanced and different amounts of these species will be attracted on the electrocatalyst surface. On the other hand, in different scan rates the transformation of Pt atoms to Pt oxides is accelerated or decelerated according to increasing or decreasing of scan rate, so in backward scan, the current of reduction of Pt oxides peak (III) to Pt and oxidation peak related to ethanol (IV) in backward scan is altered. Therefore, in low scan rates Pt oxides convert to Pt and produce enough clean Pt surface for ethanol to be oxidized and result in an increase of currents of process (III) and (IV). Whereas, in high scan rates there is not enough time for poisoning species to occupy the nanoparticle sites, so nanoparticles are clean to electrocatalyze of the ethanol molecules. Insets of C and D show the effect of scan rate on the peak potentials of different processes I and ΔE between them (D).

Same results were obtained for Pt/rGO/CCE and Pt-Cu/rGO/CCE.

Chronoamperometric study

The chronoamperometric technique was used to the study of the long-term stability of Pt/rGO/CCE, Pt-Cu/rGO/CCE, and Pt-Ni/rGO/CCE electrocatalysts in electrooxidation of ethanol. The resulted chronoamperograms in acidic solution [H_2SO_4 (0.1 M)] of ethanol (0.3 M) at 0.6 V (vs SCE), were shown in Fig. 9. For all electrocatalysts, the observed current decreased rapidly in initial times probably due to poisoning of the electrocatalyst surface active sites [78-80]. As can be seen, the rate of decreasing in the initial current for the Pt-Ni/rGO/CCE electrocatalyst is very low compared to others. Then the currents decrease gradually with time. After 1000 s, the order of the final currents is: Pt-Ni/rGO/CCE (curve c, 2.6 mA cm^{-2})>> Pt-Cu/rGO/CCE (curve b, 1.1 mA cm^{-2})> Pt/rGO/CCE (curve a, 0.85 mA cm^{-2}). Therefore, the Pt-Ni/rGO/CCE electrocatalyst shows higher current compared with Pt-Cu/rGO/CCE and Pt/rGO/CCE and demonstrates its greater long-term stability. On the other hand, these results again confirm that the addition of Ni atoms in alloy can enhance the stability and resistance to CO poisoning of Pt alloy electrocatalyst in ethanol electrooxidation. Based on the above results, it can be again concluded that Pt-Ni/rGO/CCE has the highest electrocatalytic performance.

CONCLUSIONS

Pt/rGO, Pt-Cu/rGO, and Pt-Ni/rGO nanocomposites were successfully synthesized by electrochemical method on the Carbon-Ceramic Electrode (CCE). The electrosynthesized nanocomposites were characterized by SEM, XRD, and EDX. The electrocatalytic oxidation of ethanol was studied in acidic media at the Pt/rGO/, Pt-Cu/rGO/CCE and Pt-Ni/rGO/CCE electrocatalysts. According to the obtained results of electrochemical investigations, Pt-Ni/rGO/CCE electrocatalyst present greater electrocatalytic performances toward ethanol electrooxidation compared to Pt/rGO/CCE and also Pt-Cu/rGO/CCE electrocatalysts: Pt-Ni/rGO/CCE (ECSA=25.28, Jpf=0.156 mA/cm^2, Jpf/Jpb=1.12 and E_{onset}=0.2 V), Pt-Cu/rGO/CCE (ECSA=19.09, Jpf=0.108 mA/cm^2, Jpf/Jpb=0.99 and E_{onset}=0.3 V) and Pt/rGO/CCE (ECSA=28.28, Jpf=0.092 mA/cm^2, Jpf/Jpb=0.55 and E_{onset}=0.35 V). Indeed, with the introduction of Ni atoms, the Jpf is increase, the Jpb and onset potential are decrease,

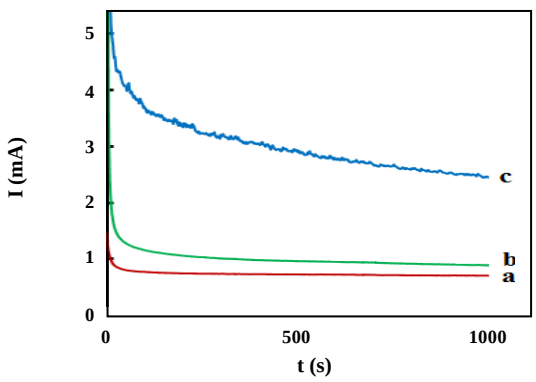

Fig. 9: Chronoamperograms of the Pt/rGO/CCE (curve a), Pt-Cu/rGO/CCE (curve b) and Pt-Ni/rGO/CCE (curve c) electrocatalysts in 0.1 M H_2SO_4 + 0.3 M ethanol solution for 1000 s (polarization potential: 0.6 V).

the ratio of Jpf/Jpb is increasing and stability is also increased, the results which indicate that the addition of Ni atoms can efficiently release CO-like carbonaceous species adsorbed on the Pt surface and increase the kinetic of ethanol electrooxidation reaction. Based on the obtained results, one can be expected that the Pt-Ni/rGO/CCE electrocatalyst is a promising system for ethanol fuel cell applications.

Acknowledgment

The authors gratefully acknowledge the Research Council of Azerbaijan Shahid Madani University for financial support.

Received : Oct. 27, 2017 ; Accepted : Apr. 12, 2018

REFERENCES

[1] Srinivasan S., Manko D.J., Koch H., Enayetullah M.A., Appleby A.J., Recent Advances in Solid Polymer Electrolyte Fuel Cell Technology with Low Platinum Loading Electrodes, *J. Power Sources*, **29**: 367-387 (1990).

[2] Naddaf E., Abedi M.R., Zabihi M.S., Imani A., Electrocatalytic Oxidation of Ethanol and Ethylene Glycol onto Poly (o-Anisidine)-Nickel Composite Electrode, *Iran. J. Chem. Chem. Eng. (IJCCE)*, **36**: 59-70 (2017).

[3] Johansson B., Security Aspects of Future Renewable Energy Systems-A Short Overview, *Energy*, **61**: 598-605 (2013).

[4] Owusu P.A., Asumadu-Sarkodie S., A Review of Renewable Energy Sources, Sustainability Issues and Climate Change Mitigation, *Cogent Engineering*, **3**: 1167990 (2016).

[5] Ong B.C., Kamarudin S.K., Basri S, Direct Liquid Fuel Cells: A Review, *Int. J. Hydrogen Energy*, **42**:10142-10157(2017).

[6] Antolini E., Pt-Ni and Pt-M-Ni (M = Ru, Sn) Anode Catalysts for Low-Temperature Acidic Direct Alcohol Fuel Cells: A Review, *Energies*, **10**: 1-20 (2017).

[7] Zalc J., Sokolovskii V., Löffler D., Are Noble metal-Based Water–Gas Shift Catalysts Practical for Automotive Fuel Processing?, *J. Catal.*, **206**: 169-171 (2002).

[8] Maya-Cornejo J., Garcia-Bernabé A., Compañ V., Bimetallic Pt-M Electrocatalysts Supported on Single-Wall Carbon Nanotubes for Hydrogen and Methanol Electrooxidation in Fuel Cells Applications, *Int. J. Hydrogen Energy*, **43**: 872-884 (2018).

[9] Osmieri L., Escudero-Cid R., Monteverde Videla A.H.A., Ocón P., Specchia S., Application of a Non-Noble Fe-N-C Catalyst for Oxygen Reduction Reaction in an Alkaline Direct Ethanol Fuel Cell, *Renewable Energy*, **115**: 226-237(2018).

[10] Zhou W.J., Hou B.Z., Zli W., Hzhou Z., Qsong S., Sun G.Q., Xin Q., Mgoula S., Tsiakaras P., Performance Comparison of Low-Temperature Direct Alcohol Fuel Cells with Different Anode Catalysts, *J. Power Sources*, **126**:16-22 (2004).

[11] Mann J., Yao N., Bocarsly A.B., Characterization and Analysis of New Catalysts for a Direct Ethanol Fuel Cell, *Langmuir*, **22**: 10432-10436 (2006).

[12] Edenhofer O., Pichs-Madruga R., Sokona Y., Seyboth K., Kadner S., Zwickel T., Eickemeier P., Hansen G., Schlömer S., Stechow von. C., "Renewable Energy Sources and Climate Change Mitigation: Special Report of the Intergovernmental Panel on Climate Change", Cambridge University Press (2011).

[13] Wang Y., Zou S., Cai W.-B., Recent Advances on Electro-Oxidation of Ethanol on Pt- and Pd-Based Catalysts: From Reaction Mechanisms to Catalytic Materials, *Catalysts*, **5**:1507-1534(2015).

[14] Navaee A., Salimi A., Anodic Platinum Dissolution, Entrapping by Amine Functionalized-Reduced Graphene Oxide: A Simple Approach to Derive the Uniform Distribution of Platinum Nanoparticles with Efficient Electrocatalytic Activity for Durable Hydrogen Evolution and Ethanol Oxidation, *Electrochim. Acta*, **211**: 322-330 (2016).

[15] Eshghi A., Kheirmend M., Surface Modification of Glassy Carbon Electrode by Ni-Cu Nanoparticles as a Competitive Electrode for Ethanol Electro-oxidation, *Iran. J. Chem. Chem. Eng. (IJCCE)*, **37**(5): 1-8 (2018).

[16] Raoof J.-B., Hosseini S.R., Mousavi-Sani S.Z., Improved Hydrogen Evolution on Glassy Carbon Electrode Modified with Novel Pt/Cetyltrimethylammonium Bromide Nanoscale Aggregates, *Chin. J. Catal.*, **36**: 216-220 (2015).

[17] Valério Neto E.S., Gomes M.A., Salazar-Banda G.R., Eguiluz K.I.B., Pt and Pt-Rh Nanowires Supported on Carbon and SnO_2:Sb Nanoparticles for Ethanol Electrochemical Oxidation in Acidic Media, *Int. J. Hydrogen Energy*, **43**:178-188(2018).

[18] Yan S.-Y., Huang Y.-R., Yang C.-Y., Liu C.-W., Wang J.-H., Wang K.-W., Enhanced Activity of Ethanol Oxidation Reaction on PtM (M=Au, Ag and Sn): The Importance of Oxophilicity and Surface Oxygen Containing Species, *Electrochim. Acta*, **259**: 733-74 1(2018).

[19] Li B., Fan H., Cheng M., Song Y., Li F., Wang X., Wang R., Porous Pt-NiO:X Nanostructures with Ultrasmall Building Blocks and Enhanced Electrocatalytic Activity for the Ethanol Oxidation Reaction, *RSC Adv.*, **8**: 698-705 (2018).

[20] Sulaiman J.E., Zhu S., Xing Z., Chang Q., Shao M., Pt-Ni Octahedra as Electrocatalysts for the Ethanol Electro-Oxidation Reaction, *ACS Catal.* **7**: 5134-5141 (2017).

[21] Sedighi M., Rostami A.A., Alizadeh E., Enhanced Electro-Oxidation of Ethanol using Pt-CeO_2 Electrocatalyst Prepared by Electrodeposition Technique, *Int. J. Hydrogen Energy*, **42**: 4998-5005 (2017).

[22] Zhang B.-W., Sheng T., Wang Y.-X., Qu X.-M., Zhang J.-M., Zhang Z.-C., Liao H.-G., Zhu F.-C., Dou S.-X., Jiang Y.-X., Sun S.-G., Platinum-Cobalt Bimetallic Nanoparticles with Pt Skin for Electro-Oxidation of Ethanol, *ACS Catal.*, **7**: 892-895(2017).

[23] Yang W.-H., Zhang Q.-H., Wang H.-H., Zhou Z.-Y., Sun S.-G., Preparation and Utilization of a Sub-5 nm PbO_2 Colloid as an Excellent co-Catalyst for Pt-Based Catalysts Toward Ethanol Electro-Oxidation, *New J. Chem.*, **41**: 12123-12130 (2017).

[24] Sánchez-Monreal J., García-Salaberri P.A., Vera M., A Genetically Optimized Kinetic Model for Ethanol Electro-Oxidation on Pt-Based Binary Catalysts used in Direct Ehanol Fuel Cells, *J. Power Sources*, **363**: 341-355 (2017).

[25] Gu X., Wang C., Yang L., Yang C., 3D Porous PtAg Nanotubes for Ethanol Electro-Oxidation, *J. Nanosci. Nanotech*, **17**:2843-2847(2017).

[26] Song H., Luo M., Qiu X., Cao G., Insights Into the Endurance Promotion of PtSn/CNT Catalysts by Thermal Annealing for Ethanol Electro-Oxidation, *Electrochim. Acta*, **213**:578-586(2016).

[27] Momeni M.M., Nazari Z., Electrodeposited Platinum Nanostructure Films on the Tantalum for Ethanol Electro-Oxidation, *Surf. Eng.*, **32**: 356-362(2016).

[28] Mikhailova A.A., Pasynskii A.A., Grinberg V.A., Velikodnyi Yu.A., Khazova O.A., CO and Methanol Oxidation at Platinum-tin Electrodes, *Russ. J. Electrochem.*, **46**: 26-33 (2010).

[29] Wang H., Jusys Z., Behm R., Ethanol Electrooxidation on a Carbon-Supported Pt Catalyst: Reaction Kinetics and Product Yields, *J. Phy. Chem. B.*, **108**:19413-19424(2004).

[30] Yoshitake T., Shimakawa Y., Kuroshima S., Kimura H., Ichihashi T., Kubo Y., Kasuya D., Takahashi K., Kokai F., Yudasaka M., Preparation of Fine Platinum Catalyst Supported on Single-Wall Carbon Nanohorns for Fuel Cell Application, *Physica B Condens. Matter*, **323**: 124-126 (2002).

[31] Sun S., Jusys Z., Behm R., Electrooxidation of Ethanol on Pt-Based and Pd-Based Catalysts in Alkaline Eectrolyte under Fuel Cell Relevant Reaction and Transport Conditions, *J. Power Sources*, **231**: 122-133 (2013).

[32] Xu C., Cheng L., Shen P., Liu Y., Methanol and Ethanol Electrooxidation on Pt and Pd Supported on Carbon Microspheres in Alkaline Media, *Electrochem. Commun.*, **9**: 997-1001 (2007).

[33] Xia Q.Q., Zhang L.Y., Zhao Z.L., Li C.M., Growing Platinum-Ruthenium-Tin Ternary alloy Nanoparticles on Reduced Graphene Oxide for Strong Ligand Effect Toward Enhanced Ethanol Oxidation Reaction, *J. Colloid Interface Sci.* **506**:135-143(2017)

[34] Kanninen P., Luong N.D., Sinh L.H., Flórez-Montaño J., Jiang H., Pastor E., Seppälä J., Kallio T., Highly Active Platinum Nanoparticles Supported by Nitrogen/Sulfur Functionalized Graphene Composite for Ethanol Electro-Oxidation, *Electrochim. Acta* **242**:315-326(2017).

[35] Samuei S., Fakkar J., Rezvani Z., Shomali A., Habibi B., Synthesis and Characterization of Graphene Quantum Dots/CoNiAllayered Double-Hydroxide Nanocomposite: Application as a Glucose Sensor, *Anal. Biochem.* **521**: 31-39 (2017).

[36] Kakaei K., Decoration of Graphene Oxide with Platinum Tin Nanoparticles for Ethanol Oxidation, *Electrochim. Acta* **165**: 330-337 (2015).

[37] Kumar R., da Silva E.T.S.G., Singh R.K., Savu R., Alaferdov A.V., Fonseca L.C., Carossi L.C., Singh A., Khandka S., Kar K.K., Alves O.L., Kubota L.T., Moshkalev S.A., Microwave-Assisted Synthesis of Palladium Nanoparticles Intercalated Nitrogen Doped Reduced Graphene Oxide and Their Electrocatalytic Activity for Direct-Ethanol Fuel Cells, *J. Colloid Interface Sci.*, **515**:160-171 (2018).

[38] Arabzadeh A., Salimi A., Ashrafi M., Soltanian S., Servati P., Enhanced Visible Light Driven Photoelectrocatalytic Oxidation of Ethanol at Reduced Graphene Oxide/CdS Nanowires Decorated with Pt Nanoparticles, *Catal. Sci. Technol.*, **6**: 3485-3496 (2016).

[39] Maya-Cornejo J., Carrera-Cerritos R., Sebastián D., Ledesma-García J., Arriaga L.G., Aricò A.S., Baglio V., PtCu Catalyst for the Electro-Oxidation of Ethanol in an Alkaline Direct Alcohol Fuel Cell, *Int. J. Hydrogen Energy*, **42**:27919-27928(2017).

[40] Wu G., Chen Y.-S., Xu B.-Q., Remarkable Support Effect of SWNTs in Pt Catalyst for Methanol Electrooxidation, *Electrochem. Commun.*, 7: 1237-1243 (2005).

[41] Sebastián D., Calderón J., González-Expósito J., Pastor E., Martínez-Huerta M., Suelves I., Moliner R., Lázaro M., Influence of Carbon Nanofiber Properties as Electrocatalyst Support on the Electrochemical Performance for PEM Fuel Cells, *Int. J. Hydrogen Energy*, **35**: 9934-9942 (2010).

[42] Solar J., Derbyshire F., De Beer V., Radovic L., Effects of Surface and Structural Properties of Carbons on the Behavior of Carbon-Supported Molybdenum Catalysts, *J. Catal.*, **129**: 330-342 (1991).

[43] Solar J., Leon C.L., Osseo-Asare K., Radovic L., On the Importance of the Electrokinetic Properties of Carbons for Their Use as Catalyst Supports, *Carbon*, **28**: 369-375(1990).

[44] Fraga M., Jordao E., Mendes M., Freitas M., Faria J., Figueiredo J., Properties of Carbon-Supported Platinum Catalysts: Role of Carbon Surface Sites, *J. Catal.* **209**:355-364(2002).

[45] Novoselov K., Geim A., The Rise of Graphene, *Nat. Mater.*, **6**:183-191(2007).

[46] Stankovich S., Dikin D.A., Dommett G.H., Kohlhaas K.M., Zimney E.J., Stach E.A., Piner R.D., Nguyen S.T., Ruoff R.S., Graphene-Based Composite Materials, *Nature* **442**:282-286(2006).

[47] Li L., Wu Y., Lu J., Nan C., Li Y., Synthesis of Pt-Ni/Graphene via in Situ Reduction and Its Enhanced Catalyst Activity for Methanol Oxidation, *Chem. Commun.* **49**:7486-7488(2013).

[48] Suh W.-k., Ganesan P., Son B., Kim H., Shanmugam S., Graphene Supported Pt-Ni Nanoparticles for Oxygen Reduction Reaction in Acidic Electrolyte, *Int. J. Hydrogen Energy* **41**: 12983-12994 (2016).

[49] Ghasemi S., Hosseini S.R., Kazemi Z., Electrochemical Deposition of Pt-Ni on Reduced Graphene Oxide as Counter Electrode Material for Dye-Sensitized Solar Cell, *J. Photochem. Photobiol.A:Chemistry* **348**: 263-268 (2017).

[50] Zhao F., Kong W., Hu Z., Liu J., Zhao Y., Zhang B., Tuning the Performance of Pt-Ni Alloy/Reduced Graphene Oxide Catalysts for 4-Nitrophenol Reduction, *RSC Adv.* **6**:79028-79036(2016).

[51] Seger B., Kamat P.V., Electrocatalytically Active Graphene-Platinum Nanocomposites. Role of 2-D Carbon Support in PEM fuel cells, *J. Phys. Chem. C.* **113**:7990-7995(2009).

[52] Yoo E., Okata T., Akita T., Kohyama M., Nakamura J., Honma I., Enhanced Electrocatalytic Activity of Pt Subnanoclusters on Graphene Nanosheet Surface, *Nano Letters.*, **9**: 2255-2259 (2009).

[53] Dong L., Gari R.R.S., Li Z., Craig M.M., Hou S., Graphene-Supported Platinum and Platinum-Ruthenium Nanoparticles with High Electrocatalytic Activity for Methanol and Ethanol Oxidation, *Carbon*, **48**: 781-787 (2010).

[54] Das D., Basumallick I., Ghosh S., Methanol and Ethanol Electro-oxidation on to Platinum Loaded Reduced Graphene Oxide Surface for Fuel Cell Application, *Br. J. Appl. Sci. Technol.*, **7**: 630-641 (2015).

[55] Shen Y., Xiao K., Xi J., Qiu X., Comparison study of Few-Layered Graphene Supported Platinum and Platinum Alloys for Methanol and Ethanol Electro-Oxidation, *J.Power Sources*, **278**: 235-244 (2015).

[56] Qian W., Hao R., Zhou J., Eastman M., Manhat B.A., Sun Q., Goforth A.M., Jiao J., Exfoliated Graphene-Supported Pt and Pt-Based Alloys as Electrocatalysts for Direct Methanol Fuel Cells, *Carbon*, **52**: 595-604 (2013).

[57] Zhou Y.-G., Chen J.-J., Wang F.-b., Sheng Z.-H., Xia X.-H., A Facile Approach to the Synthesis of Highly Electroactive Pt Nanoparticles on Graphene as an Anode Catalyst for Direct Methanol Fuel Cell, *Chem. Commun.*, **46**: 5951-5953 (2010).

[58] Hu Y., Wu P., Zhang H., Cai C., Synthesis of Graphene-Supported Hollow Pt-Ni Nanocatalysts for Highly Active Electrocatalysis Toward the Methanol Oxidation Reaction, *Electrochim. Acta*, **85**: 314-321 (2012).

[59] Hu Y., Wu P., Yin Y., Zhang H., Cai C., Effects of Structure, Composition, and Carbon Support Properties on the Electrocatalytic Activity of Pt-Ni-Graphene Nanocatalysts for the Methanol Oxidation, *Appl. Catal. B: Environ.*, **111**: 208-217 (2012).

[60] Habibi B., Dadashpour E., Carbon-Ceramic Supported Bimetallic Pt-Ni Nanoparticles as an Electrocatalyst for Electrooxidation of Methanol and Ethanol in Acidic Media, *Int. J. Hydrogen Energy*, **38**: 5425-5434 (2013).

[61] Li F., Guo Y., Chen M., Qiu H., Sun X., Wang W., Liu Y., Gao J., Comparison study of Electrocatalytic Activity of Reduced Graphene Oxide Supported Pt-Cu Bimetallic or Pt Nanoparticles for the Electrooxidation of Methanol and Ethanol, *Int. J. Hydrogen Energy*, **38**:14242-14249 (2013).

[62] Habibi B., Delnavaz N., Pt-CeO_2/Reduced Graphene Oxide Nanocomposite for the Electrooxidation of Formic Acid and Formaldehyde, *RSC Adv.*, **5**: 73639-73650 (2015).

[63] Hummers Jr W.S., Offeman R.E., Preparation of Graphitic Oxide, *J. Am. Chem. Soc.*, **80**: 1339-1339 (1958).

[64] Chen L., Tang Y., Wang K., Liu C., Luo S., Direct Electrodeposition of Reduced Graphene Oxide on Glassy Carbon Electrode and Its Electrochemical Application, *Electrochem. Commun.*, **13**: 133-137 (2011).

[65] Habibi B., Delnavaz N., Carbon-Ceramic Supported Bimetallic Pt-Ni Nanoparticles as an Electrocatalyst for Oxidation of Formic Acid, *Int. J. Hydrogen Energy*, **36**: 9581-9590 (2011).

[66] Habibi B., Delnavaz N., Electrosynthesis, Characterization and Electrocatalytic Properties of Pt-Sn/CCE Towards Oxidation of Formic Acid, *RSC Adv.*, **2**: 1609-1617 (2012).

[67] Almeida T.S., Kokoh K.B., Andrade A.R.De, Effect of Ni on Pt/C and PtSn/C Prepared by the Pechini Method, *Int. J. Hydrogen Energy*, **36**: 3803-3810 (2011).

[68] Arul Dhas N., Paul Raj C., Gedanken A., Synthesis, Characterization, and Properties of Metallic Copper Nanoparticles, *Chem. Mater.*, **105**: 1446-1452 (1998).

[69] Wang Z., Du Y., Zhang F., Zheng Z., Zhang Y., Wang C., High Electrocatalytic Activity of Non-Noble Ni-Co/Graphene Catalyst for Direct Ethanol Fuel Cells, *J. Solid State Electrochem.*, **17**: 99-107 (2013).

[70] Pournaghi-Azar M., Habibi-A B., Preparation of a Platinum Layer-Modified Aluminum Electrode by Electrochemical and Electroless Cementations and Its Use for the Electrooxidation of Methanol, *J. Electroanal. Chem.*, **580**: 23-34 (2005).

[71] Trasatti S., Petrii O., Real Surface Area Measurements in Electrochemistry, *J. Electroanal. Chem.*, **327**: 353-376 (1992).

[72] Croissant M., Napporn T., Léger J.-M., Lamy C., Electrocatalytic Oxidation of Hydrogen at Platinum-Modified Polyaniline Electrodes, *Electrochim. Acta*, **43**: 2447-2457 (1998).

[73] De Souza J., Queiroz S., Bergamaski K., Gonzalez E., Nart F., Electro-Oxidation of Ethanol on Pt, Rh, and PtRh Electrodes. A Study Using DEMS and In-Situ FTIR Techniques, *J. Phys. Chem. B.*, **106**: 9825-9830 (2002).

[74] Iwasita T., Rasch B., Cattaneo E., Vielstich W., A Sniftirs Study of Ethanol Oxidation on Platinum, *Electrochim. Acta*, **34**: 1073-1079 (1989).

[75] Razmi H., Habibi E., Heidari H., Electrocatalytic Oxidation of Methanol and Ethanol at Carbon Ceramic Electrode Modified with Platinum Nanoparticles, *Electrochim. Acta*, **53**: 8178-8185 (2008).

[76] Lamy C., Belgsir E., Leger J., Electrocatalytic Oxidation of Aliphatic Alcohols: Application to the Direct Alcohol Fuel Cell (DAFC), *J. Appl. Electrochem.*, **31**: 799-809 (2001).

[77] Hitmi H., Belgsir E., Léger J.-M., Lamy C., Lezna R., A Kinetic Analysis of the Electro-Oxidation of Ethanol at a Platinum Electrode in Acid Medium, *Electrochim. Acta*, **39**: 407-415 (1994).

[78] Sen Gupta S., Singh S., Datta J., Temperature Effect on the Electrode Kinetics of Ethanol Electro-Oxidation on Sn Modified Pt Catalyst Through Voltammetry and Impedance Spectroscopy, *Mater. Chem. Phys.*, **120**:682-690(2010).

[79] Ren F., Wang H., Zhai C., Zhu M., Yue R., Du Y., Yang P., Xu J., Lu W., Clean Method for the Synthesis of Reduced Graphene Oxide-Supported PtPd Alloys with High Electrocatalytic Activity for Ethanol Oxidation in Alkaline Medium, *ACS Appl. Mater. Interfaces*, **6**: 3607-3614 (2014).

[80] Bin D., Ren F., Wang H., Zhang K., Yang B., Zhai C., Zhu M., Yang P., Du Y., Facile Synthesis of PVP-Assisted PtRu/RGO Nanocomposites with High Electrocatalytic Performance for Methanol Oxidation, *RSC Adv.*, **4**: 39612-39618 (2014).